PHYSICAL REVIEW A **73**, 021603(R) (2006)

Sound propagation in elongated superfluid fermionic clouds

P. Capuzzi,* P. Vignolo,† F. Federici,‡ and M. P. Tosi§
NEST-CNR-INFM and Classe di Scienze, Scuola Normale Superiore, I-56126 Pisa, Italy
(Received 12 September 2005; published 27 February 2006)

We use hydrodynamic equations to study sound propagation in a superfluid Fermi gas at zero temperature inside a strongly elongated cigar-shaped trap, with main attention to the transition from the BCS to the unitary regime. First, we treat the role of the radial density profile in the limit of a cylindrical geometry and then evaluate numerically the effect of the axial confinement in a configuration in which a hole is present in the gas density at the center of the trap. We find that in a strongly elongated trap the speed of sound in both the BCS and the unitary regime differs by a factor $\sqrt{3/5}$ from that in a homogeneous three-dimensional superfluid. The predictions of the theory could be tested by measurements of sound-wave propagation in a setup such as that exploited by Andrews *et al.* [Phys. Rev. Lett. **79**, 553 (1997)] for an atomic Bose-Einstein condensate.

DOI: 10.1103/PhysRevA.73.021603 PACS number(s): 03.75.Kk, 03.75.Ss, 47.37.+q

Strong evidence for a superfluid state in ultracold Fermi gases near a Feshbach resonance has come from experimental studies using as probes ballistic expansion [1,2], collective modes [3,4], rf spectroscopy [5], and the generation of quantized vortices [6]. Since the BCS weak-coupling limit and the unitary strong-coupling limit are characterized by the same collective-mode frequencies and expansion dynamics [7], attention has been drawn to probes such as the cloud-size measurements [8], rf spectroscopy, critical temperature measurements, and the study of sound-wave propagation as allowing a clear identification of these two regimes. In particular Ho [9] and Heiselberg [10] have evaluated the speed of first and second sound in a homogeneous Fermi superfluid as functions of the coupling regime. At low temperature the first sound velocity is given by $u_1 = v_F\sqrt{[1+(2/\pi)\hbar k_F a]/3} \simeq v_F/\sqrt{3}$ in the dilute BCS limit and by $u_1 \simeq 0.37 v_F$ in the unitary limit. Here v_F and k_F are the Fermi velocity and wave number, while a is the s-wave scattering length.

The main purpose of this paper is to evaluate the propagation of density perturbations in a superfluid Fermi gas at zero temperature as a function of coupling strength in an experimentally realizable setup. This simulates the setup used in the experiments of Andrews *et al.* [11] on the propagation of sound pulses along the axis of an elongated cloud of Bose-Einstein condensed ^{23}Na atoms. In their experiments a density perturbation is generated by turning on a laser at the center of the trap and two pulses propagate in opposite directions along the trap axis. We describe the dynamics of density fluctuations in the superfluid by hydrodynamic equations, namely the continuity equation

$$\partial_t n + \nabla \cdot (n\mathbf{v}) = 0, \tag{1}$$

and the Euler equation

$$m\partial_t \mathbf{v} + \nabla\left[\mu(n) + V(\mathbf{r}) + \tfrac{1}{2}m\mathbf{v}^2\right] = 0 \tag{2}$$

for the time-dependent density profile $n(\mathbf{r},t)$ and velocity field $\mathbf{v}(\mathbf{r},t)$ of the trapped gas. The equation of state enters through the density-dependent chemical potential $\mu(n)$, and $V(\mathbf{r})$ describes the external potentials. The laser beam is simulated in our study by a time-independent effective potential $U(z) = U_0 e^{-z^2/w^2}$ having amplitude U_0 and width w, which is turned on at the center of the trap.

The cylindrical configuration. We discuss first the cylindrical configuration case corresponding to $V(\mathbf{r}) = m\omega_\perp^2 r_\perp^2/2$, where $\omega_\perp$ is the radial trap frequency. This is amenable to analytical treatment. The equilibrium density $n_0(r_\perp)$ is determined from the relation $\mu(n_0) = \bar{\mu} - m\omega_\perp^2 r_\perp^2/2$, where $\bar{\mu}$ is determined by the normalization condition $\int n_0(r_\perp) d^2 r_\perp = \tilde{n}$, $\tilde{n}$ being the linear density. Linearization around equilibrium sets $n(\mathbf{r},t) = n_0 + \delta n(r_\perp) e^{i(\omega t - qz)}$ and $\mu(n) = \mu(n_0) + \partial\mu/\partial n|_{n=n_0} \delta n(r_\perp) e^{i(\omega t - qz)}$. Thus Eqs. (1) and (2) lead to the eigenvalue equation

$$m\omega^2 \delta n = q^2\left(n_0\, \partial\mu/\partial n|_{n=n_0}\delta n\right) - \nabla_\perp \cdot \left[n_0 \nabla_\perp \left(\partial\mu/\partial n|_{n=n_0}\delta n\right)\right] \tag{3}$$

and integration in the (x,y) plane yields the dispersion relation

$$\omega = q\left(\frac{1}{m}\int n_0\, \partial\mu/\partial n|_{n=n_0}\delta n d^2 r_\perp \Big/ \int \delta n d^2 r_\perp\right)^{1/2}. \tag{4}$$

The lowest collective mode of the gas is obtained by taking δn as the lowest-energy solution of Eq. (3) with $q=0$, i.e., $\delta n(r_\perp) \propto (\partial\mu/\partial n|_{n=n_0})^{-1}$. Therefore the sound velocity is

$$u_1 = \left(\frac{1}{m}\int n_0 d^2 r_\perp \Big/ \int \left(\partial\mu/\partial n|_{n=n_0}\right)^{-1} d^2 r_\perp\right)^{1/2}. \tag{5}$$

Equation (5) applies to all gases in cylindrical geometries which can be described by hydrodynamic equations.

For a power-law form of the equation of state, $\mu(n) = \mathcal{C} n^\gamma$, the equilibrium density profile takes the explicit

*Electronic address: capuzzi@sns.it
†Electronic address: vignolo@sns.it
‡Electronic address: fr.federici@sns.it
§Electronic address: tosim@sns.it

 ©2006 The American Physical Society

form $n_0(r_\perp)=(\bar{\mu}/\mathcal{C})^{1/\gamma}(1-r_\perp^2/R_{\rm TF}^2)^{1/\gamma}$ where $R_{\rm TF}=\sqrt{2\bar{\mu}/m\omega_\perp^2}$ is the radial size of the cloud. Equation (5) then reduces to

$$u_1^2=\frac{\gamma\bar{\mu}}{(1+\gamma)m}. \tag{6}$$

For $\gamma=1$, Eq. (6) gives the speed of sound pulses propagating along the axis of a cylindrical condensate of bosonic atoms [12] or of molecular bosons formed by pairs of fermionic atoms. In the latter case, the mixture approaches the Bose-Einstein condensation (BEC) limit with a sound velocity $u_{\rm BEC}=(\pi n_0 a_M/2)^{1/2}\hbar/m$, with $a_{\rm M}$ the molecular scattering length $a_M\simeq 0.6a$ [13]. For a Fermi gas in the BCS ($k_{\rm F}|a|\ll 1$) and the unitary ($k_{\rm F}|a|\gg 1$) regime the equation of state is, instead, proportional to the Fermi energy $(\hbar^2/2m)(3\pi^2 n)^{2/3}$, so that $\gamma=2/3$ and $u_1=\sqrt{2\bar{\mu}/5m}$. In the former limit at very low temperatures $\bar{\mu}=mv_{\rm F}^2/2$ and $u_1=v_{\rm F}/\sqrt{5}$, while in the latter $\bar{\mu}=m(1+\beta)v_{\rm F}^2/2$ with β being a negative constant as a consequence of the strong attractive interactions as previously evaluated in several approaches [14]. In fact, because of the attraction between the two components, one component drags the other along, causing the perturbation to slow down with respect to the noninteracting case. Quantum Monte Carlo calculations find $\beta\simeq -0.57$ [15,16] and then $u_1\simeq 0.29v_{\rm F}$. These velocities thus differ by a factor $\sqrt{3/5}$ from those in the homogeneous Fermi gas [10] and would be measured in a sound propagation experiment through the central portion of a strongly elongated trap. It is worth noticing that these results differ from what a one-dimensional (1D) calculation would predict: in the latter it is straightforward to show that $u_1=\sqrt{\gamma\bar{\mu}/m}$, i.e., $u_1=v_{\rm F}$ for a strictly 1D hydrodynamic Fermi gas.

At intermediate couplings, when $k_{\rm F}|a|$ is finite, $\mathcal{C}$ depends on the density, and several forms of the equation of state have been proposed [14,17,18]. A possible solution is to use again a power law with an effective exponent γ, which may be inferred from a measured collective mode frequency [7]. The effective value of $\mathcal{C}$ can instead be determined from the cloud size. In this work we focus on a gas with a negative scattering length and choose the equation of state given by Heiselberg in the Galitskii approximation [14]. This is

$$\mu(n)=\frac{\hbar^2}{2m}(3\pi^2 n)^{2/3}\left[1+\frac{c_1 n^{1/3}}{1-c_2 n^{1/3}}\left(2+\frac{c_2 n^{1/3}}{3(1-c_2 n^{1/3})}\right)\right], \tag{7}$$

with $c_1=2a/(9\pi)^{1/3}$ giving the mean-field contribution and $c_2=6[11-2\ln 2](3\pi^2)^{1/3}a/(35\pi)$ the second-order contribution from the ladder diagrams, which takes into account the opening of the superfluid gap. Equation (7) reproduces the result $\mu=m[1+4ak_{\rm F}/(3\pi)]v_{\rm F}^2/2$ in the limit of a dilute system, and is approximately valid at intermediate densities in the unitary limit where it gives $m(1+\beta)v_{\rm F}^2/2$. The ratio between c_1 and c_2 in this case yields $\beta\simeq -0.67$. The results for the sound velocity as obtained from a self-consistent evaluation of the chemical potential and of the equilibrium density are shown in Fig. 1. In this calculation, we have taken a linear density $\tilde{n}$ corresponding to the chemical potential of 2×10^3 fermions in a cigar-shaped confinement with trap frequencies $\omega_\perp=100\ {\rm s}^{-1}$ and $\omega_z=6.3\ {\rm s}^{-1}$ (see below). The BCS and unitary limits are recovered for $a\to 0^-$ and $a\to -\infty$, respectively. The dashed line in Fig. 1 shows the sound velocity obtained within the mean-field model for a dilute Fermi gas by setting $c_2=0$ in Eq. (7). The mean-field model well describes the BCS limit, but as the coupling increases it predicts a strong drop of the sound velocity heralding collapse. The location and width of the transition from the BCS to the unitary regime are determined by the system parameters.

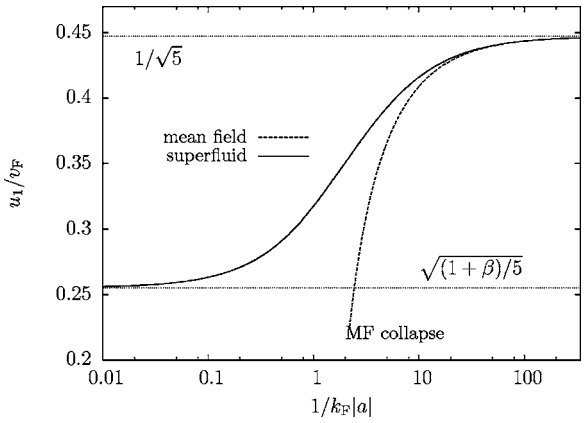

FIG. 1. Speed of sound u_1 in a cylindrical Fermi gas (in units of the Fermi velocity $v_{\rm F}$) as a function of $1/k_{\rm F}|a|$ (on a logarithmic scale). The full and the dashed lines are the results from the equation of state, (7), and from the mean-field (MF) model, respectively. The dot-dashed lines mark the BCS (upper) and the unitary (lower) limits.

Effect of axial potentials. A weak harmonic confinement along the z direction induces a smooth inhomogeneity in the axial density profile, which can be treated within a local density approximation. Assuming again a power-law equation of state, Eq. (5) leads to the velocity field

$$v_1(z)=\left(\frac{\bar{\mu}}{m}\frac{\gamma}{1+\gamma}\right)^{1/2}\left(1-\frac{z^2}{Z_{\rm TF}^2}\right)^{1/2}, \tag{8}$$

with $Z_{\rm TF}=\sqrt{2\bar{\mu}/m\omega_z^2}$, which corresponds to an oscillatory motion with frequency $\omega=\omega_z/\sqrt{2+2/\gamma}$ and velocity u_1 at the center of the trap. Even though u_1 depends on $\mathcal{C}$, the oscillation frequency is the same in the BCS and in the unitary limit, since the product between the wave number $q\propto 1/Z_{\rm TF}\propto\sqrt{1/\bar{\mu}}$ and the velocity $u_1\propto\sqrt{\bar{\mu}}$ does not depend on the chemical potential.

We next carry out a numerical study of sound propagation using the hydrodynamic Eqs. (1) and (2) in a setup simulating that used in the experiments of Andrews *et al.* [11]. In addition to radial and axial confinements provided by a strongly elongated harmonic trap, we switch on a hole-digging potential $U(z)$ at the center of the trap. The atoms are thereby expelled into two density perturbations that travel towards the ends of the trap. Since the perturbation velocity is mainly in the z direction and imaging techniques will provide column densities, we focus on the evolution of the radially integrated density profile $\tilde{n}(z)$. The numerical calculations are carried out for a system of $N=2\times 10^3$ ^{40}K atoms equally distributed in two spin-polarized states, with trap fre-

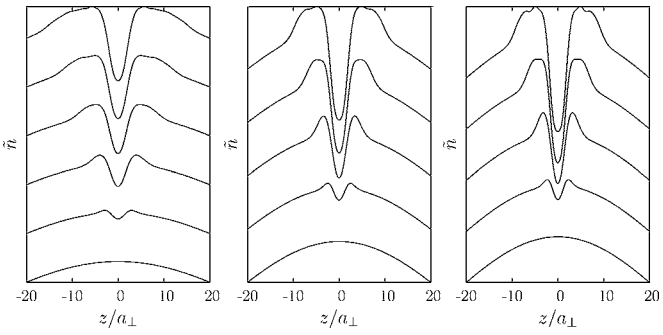

FIG. 2. Integrated density profile $\tilde{n}$ (in arbitrary units) as a function of axial coordinate z (in units of $a_\perp=[\hbar/(m\omega_\perp)]^{1/2}$) at different times starting from the bottom at $t=0$ and increasingly separated by $1.5/\omega_\perp$. The left, middle, and right panel correspond to $a/a_0=-80$, -10^5, and -10^6. For the sake of visibility the plotting range is smaller than the full extent of the density profile.

quencies $\omega_\perp=100\ \mathrm{s}^{-1}$ and $\omega_z=6.3\ \mathrm{s}^{-1}$. The potential $U(z)$ has a width w equal to 5% of the axial width of the density profile and an amplitude U_0 of magnitude up to $\hbar\omega_z$. In Fig. 2 we illustrate the time evolution of $\tilde{n}(z)$ for three values of the scattering length, $a=-80$, -10^5, and -10^6 Bohr radii. The size of the cloud decreases on increasing the coupling strength and at the same time the speed of the density perturbation also decreases.

From the evolution of the integrated density we calculate the mean velocity $\langle v_z\rangle$ of the perturbation in a time interval $\Delta t=5/\omega_\perp$. The results for $\langle v_z\rangle$ as a function of the coupling strength and for two amplitudes of the perturbing potential are shown in Fig. 3. The comparison is also illustrated between the case with $\lambda\equiv\omega_z/\omega_\perp\simeq 0.06$ and that with $\lambda=0.01$ at the same zero-coupling Fermi velocity. For weak perturbations (for example $U_0=0.16\hbar\omega_z$, full symbols in Fig. 3), giving δn of the order of a few percent of the equilibrium density at the trap center, the speed of sound for both values of λ is found to be in good agreement with the theoretical

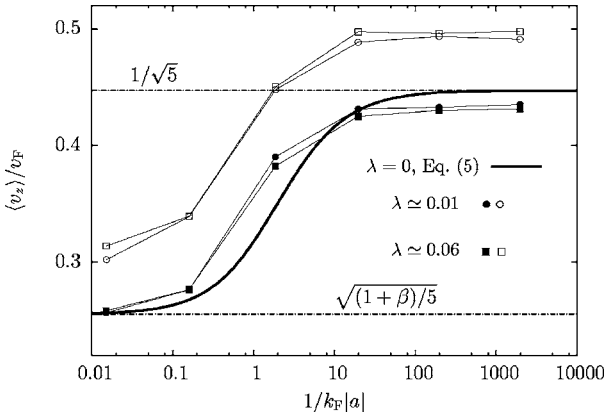

FIG. 3. Sound velocity in a superfluid Fermi gas as a function of $1/k_F|a|$ (on a logarithmic scale). Circles and squares correspond to the average speed of perturbations propagating in a trap with $\lambda\simeq 0.06$ and $\lambda=0.01$. Empty and full symbols refer to $U_0/\hbar\omega_z=0.8$ and 0.16, respectively. The thick solid line is from Eq. (5), and the dot-dashed lines mark the BCS (upper) and unitary (lower) limits. The thin solid lines are guides to the eye.

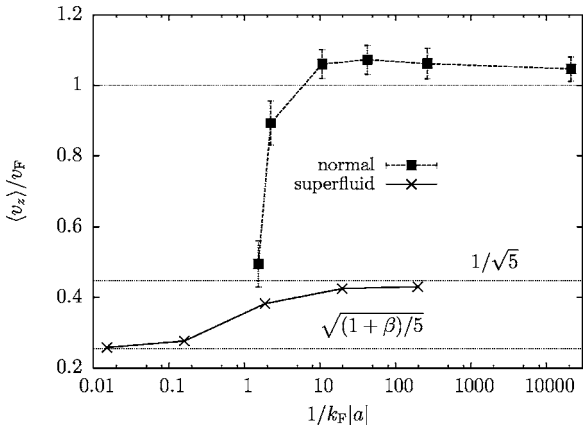

FIG. 4. Sound velocity in an elongated trap as a function of $1/k_F|a|$ (on a logarithmic scale). Circles and squares are for a superfluid at $T=0$ and for a normal Fermi gas at $T=0.2T_F$, respectively. The error bars for the normal-gas results are from the standard deviation in the velocity distributions. The dot-dashed lines show the zero-sound, the BCS, and the unitary limits, from top to bottom.

prediction given in Eq. (5) for the cylindrical gas (thick, solid line). The slight difference seen in Fig. 3 may be accounted for by the effect of the weak confinement causing the speed of sound to decrease while the density perturbation moves away from the central region of the trap [see Eq. (8)]. Beyond the perturbative regime (empty symbols in Fig. 3, referring to $U_0=0.8\hbar\omega_z$ and $\delta n/n_0\sim 20\%$) we find an upward shift of the mean velocity as a result of the increase in the local density. The overall behavior of $\langle v_z\rangle$ is still the same as in the perturbative regime. The ratio between the values at zero and large $|a|$ is about 0.61, to be compared with $\sqrt{1+\beta}\simeq 0.57$ for both the gas with $\lambda=0$ and the homogeneous gas.

Finally, we compare in Fig. 4 the sound velocity for $\lambda\simeq 0.06$ in a superfluid Fermi gas at $T=0$ with that in a normal Fermi gas at a temperature $T=0.2T_F$, T_F being the Fermi temperature at zero coupling. The dynamics of the normal gas has been studied by the Vlasov-Landau kinetic equations [19] for the one-body distribution functions of the two species, and within this framework any pairing is neglected. Our method involves binary collisions between the particles and includes Pauli-blocking effects. At low coupling the normal Fermi mixture is in the collisionless zero-sound regime and sound propagation is associated with an anisotropic deformation of the Fermi surface, the zero-sound velocity being close to v_F as shown in Fig. 4. With increasing attractions the velocity of the perturbation drops. This drop occurs at about $a\simeq -10^4 a_0$ corresponding to $1/k_F|a|\sim 1.5$, and can be attributed to both the transition towards the first-sound velocity $v_F/\sqrt{5}$ and the instability of the approaching collapse of the normal state. The transition to the superfluid state restores stability. As the transition point depends on the collisionality of the system, by increasing the number of particles we expect the drop to occur at $a>-10^4 a_0$ although the overall behavior of the transition remains the same.

In summary, we have studied sound propagation in a superfluid Fermi gas confined inside a strongly elongated har-

monic trap. We have found that the sound velocity diminishes as the superfluid goes from the BCS to the unitary regime on increasing the strength of the attractions between the atoms, and that in both limits the speed of sound differs by a factor $\sqrt{3/5}$ from that in the superfluid three-dimensional gas. The numerical study of the superfluid gas dynamics in a weak axial confinement shows that the value of the speed of sound around in the central region of the trap is close to that in the cylindrical gas. However, in situations of experimental relevance, a density perturbation of order 20% could give rise to upward shifts of the speed of sound by 10–12 %. These effects could be observed in experimental setups of trapped superfluid Fermi gases and thereby provide further insight in their superfluid state.

This work was partially supported by an Advanced Research Initiative of Scuola Normale Superiore di Pisa.

[1] C. A. Regal, M. Greiner, and D. S. Jin, Phys. Rev. Lett. **92**, 040403 (2004).
[2] M. W. Zwierlein, C. A. Stan, C. H. Schunck, S. M. F. Raupach, A. J. Kerman, and W. Ketterle, Phys. Rev. Lett. **92**, 120403 (2004).
[3] J. Kinast, S. L. Hemmer, M. E. Gehm, A. Turlapov, and J. E. Thomas, Phys. Rev. Lett. **92**, 150402 (2004).
[4] M. Bartenstein, A. Altmeyer, S. Riedl, S. Jochim, C. Chin, J. H. Denschlag, and R. Grimm, Phys. Rev. Lett. **92**, 203201 (2004).
[5] C. Chin, M. Bartenstein, A. Altmeyer, S. Riedl, S. Jochim, J. H. Denschlag, and R. Grimm, Science **305**, 1128 (2004).
[6] M. W. Zwierlein, J. R. Abo-Shaeer, A. Schirotzek, C. H. Schunck, and W. Ketterle, Nature (London) **435**, 1047 (2005).
[7] H. Hu, A. Minguzzi, X.-J. Liu, and M. P. Tosi, Phys. Rev. Lett. **93**, 190403 (2004).
[8] M. Bartenstein, A. Altmeyer, S. Riedl, S. Jochim, C. Chin, J. H. Denschlag, and R. Grimm, Phys. Rev. Lett. **92**, 120401 (2004).
[9] T.-L. Ho, Phys. Rev. Lett. **92**, 090402 (2004).
[10] H. Heiselberg, Phys. Rev. A **73**, 013607 (2006); cond-mat/0409077.
[11] M. R. Andrews, D. M. Kurn, H.-J. Miesner, D. S. Durfee, C. G. Townsend, S. Inouye, and W. Ketterle, Phys. Rev. Lett. **79**, 553 (1997).
[12] G. M. Kavoulakis and C. J. Pethick, Phys. Rev. A **58**, 1563 (1998).
[13] D. S. Petrov, C. Salomon, and G. V. Shlyapnikov, Phys. Rev. Lett. **93**, 090404 (2004).
[14] H. Heiselberg, Phys. Rev. A **63**, 043606 (2001).
[15] J. Carlson, S. Y. Chang, V. R. Pandharipande, and K. E. Schmidt, Phys. Rev. Lett. **91**, 050401 (2003); S. Y. Chang, V. R. Pandharipande, J. Carlson, and K. E. Schmidt, Phys. Rev. A **70**, 043602 (2004).
[16] G. E. Astrakharchik, J. Boronat, J. Casulleras, and S. Giorgini, Phys. Rev. Lett. **93**, 200404 (2004).
[17] P. Pieri, L. Pisani, and G. C. Strinati, Phys. Rev. B **72**, 012506 (2005).
[18] H. Hu, X.-J. Liu, and P. D. Drummond, cond-mat/0506046.
[19] Z. Akdeniz, P. Vignolo, and M. P. Tosi, Phys. Lett. A **311**, 246 (2003); F. Toschi, P. Capuzzi, S. Succi, P. Vignolo, and M. P. Tosi, J. Phys. B **37**, S91 (2004).